

Full control of magnetism in a manganite bilayer by ferroelectric polarization

Shuai Dong^{1,2,3} and Elbio Dagotto^{2,3}

¹Department of Physics, Southeast University, Nanjing 211189, China

²Department of Physics and Astronomy, University of Tennessee, Knoxville, Tennessee 37996, USA

³Materials Science and Technology Division, Oak Ridge National Laboratory, Oak Ridge, Tennessee 37831, USA

(Received 12 April 2013; revised manuscript received 8 September 2013; published 11 October 2013)

An oxide heterostructure made of manganite bilayers and ferroelectric perovskites is predicted to lead to the full control of magnetism when switching the ferroelectric polarizations. By using asymmetric polar interfaces in the superlattices, more electrons occupy the Mn layer at the *n*-type interface side than at the *p*-type side. This charge disproportionation can be enhanced or suppressed by the ferroelectric polarization. Quantum model and density functional theory calculations reach the same conclusion: a ferromagnetic-ferrimagnetic phase transition with maximal change >90% of the total magnetization can be achieved by switching the polarization's direction. This function is robust and provides full control of the magnetization's magnitude, not only its direction, via electrical methods.

DOI: 10.1103/PhysRevB.88.140404

PACS number(s): 77.55.Nv, 75.25.Dk, 75.70.Cn

Introduction. The control of magnetism using electric fields is a scientifically challenging and technologically important subject that has attracted considerable attention in recent years. Compared with single-phase multiferroics (MFE), which typically have a relatively poor performance, composite systems based on oxide heterostructures involving ferroelectric (FE) (or MFE) and ferromagnetic (FM) materials provide more practical alternatives.^{1–3} For example, by using antiferromagnetic (AF) MFE layers (e.g., BiFeO₃, Cr₂O₃, YMnO₃, etc.), the exchange bias in FM materials attached to the heterostructure can be modulated by the FE *P*'s or domains.^{4–10} In addition, in heterostructures magnetic anisotropies can be tuned by electrical methods, and currents in tunneling magnetic junctions can be affected by the FE barrier layers that also manifest as interfacial magnetoelectricity.^{11–16} Despite their success, from the fundamental viewpoint these controls of magnetism are relatively “weak” effects since the magnetic orders/moments themselves do not change substantially but only their easy axes or domain structures are rotated and tuned.

Alternatively, by using the emergent properties of correlated electronic materials, more dramatic magnetoelectric (ME) effects could be envisioned in oxide heterostructures.¹⁷ For example, in FE-La_{1–*x*}Sr_{*x*}MnO₃ (LSMO) heterostructures, experiments have found giant changes in conductances triggered by switchable FE *P*'s.^{18–22} The associated physical mechanism is believed to be the modulation by the FE field effect of the local electronic density in manganites near the interfaces (see Fig. 1).^{23–26} However, typically this effect can only penetrate no more than three unit cells (u.c.) in manganites before the effect is almost fully screened.^{23–26} Then, the proposed magnetic phase transitions occur only within a few interfacial layers, inducing a relatively small modification of the total magnetization (*M*).^{18–22}

Another issue of much relevance in oxide heterostructures is the polar discontinuity, which is emphasized for interfaces between insulators (e.g., LaAlO₃-SrTiO₃).²⁸ But this effect is often neglected in heterostructures with conductive components, e.g., LSMO, since it will be screened within a few u.c. similar to that in the FE field effect.

Model system. In this Rapid Communication, by reducing the thickness of the manganite component to bilayer size, both

the FE field effect and polar discontinuity become prominent despite the metallicity of the manganite. A direct advantage of bilayers is the maximized interface/volume ratio (up to 100%) for manganites that allows each manganite layer to be fully controlled by the FE *P*. More importantly, the neighboring asymmetric polar interfaces break the symmetry of the FE field effect in periodic superlattices (SLs), conceptually different from results in symmetric interfaces in SLs or single interfaces in simple heterostructures. The asymmetric design and ultrathin bilayers are crucial to achieving the full control of magnetism reported in our study.

As our model system, SLs stacked along the conventional (001) direction made of $R_{1-x}A_x\text{MnO}_3\text{-}D\text{TiO}_3$ (*D* = divalent cation, *R* = trivalent rare-earth metal, and *A* = divalent alkaline-earth metal) are here considered, as sketched in Fig. 2(a). The manganite components are thin involving only bilayers while the FE titanate is assumed to be slightly thicker to maintain its *P*.²⁰ Asymmetric polar interfaces are used: the interfaces with TiO₂- $R_{1-x}A_x\text{O-MnO}_2$ and TiO₂-*DO*-MnO₂ will be referred to as *n*-type and *p*-type interfaces, respectively. The *n*-type interface, with a positively charged ($R_{1-x}A_x\text{O}$)^{(1–*x*)+} layer, will attract electrons to its nearest-neighbor (NN) MnO₂ layer, while the *p*-type interface will repel electrons away from the interface. Therefore, even without ferroelectricity the asymmetric interfaces already modulate the electronic density and electrostatic potential within the manganite bilayers.

When the FE *P* points to the *n*-type interface (the +*P* case), the electrostatic potential difference between the two MnO₂ layers will be further split, thus enhancing the charge disproportionation. However, when the FE *P* points to the *p*-type interface (the –*P* case) the electrostatic potential from the polar interfaces will be partially compensated, thus suppressing the electronic disproportionation. The above processes are summarized in Fig. 2(b). In the ideal limit of the –*P* case, if these two effects (asymmetric polar interfaces vs FE *P*) could be fully balanced, both the electrostatic potential and electronic distribution in the manganite bilayers would become uniform. By suitable combinations of couplings, this nearly full compensation is possible since a robust FE perovskite (e.g., PbZr_{*y*}Ti_{1–*y*}O₃ or Ba_{1–*y*}Sr_{*y*}TiO₃) has a large *P*, which is

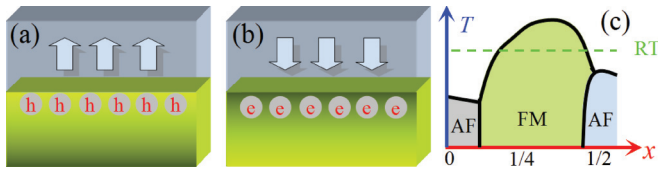


FIG. 1. (Color online) (a),(b) Sketch of FE-field effect. Arrows denote the FE P 's. Holes and electrons are attracted to the interfaces in (a) and (b), respectively. (c) A simplified phase diagram of LSMO.²⁷ x : doping concentration; T : temperature; RT: room- T . The FM region is sandwiched between two AF regions.

equivalent to a surface charge of 0.1–1 electrons per u.c. that can be tuned by adjusting the concentration y to fit the polar charge $(R_{1-x}A_xO)^{(1-x)+}$ which is very similar in magnitude. Below, this ideal $-P$ case limit is adopted in the model simulations [with a FE surface charge $(1-x)/2$ electrons per u.c.] to achieve a clear physical scenario and magnify contrasting effects when compared with the $+P$ case. Deviations from this ideal limit lead to qualitatively similar results in practice.

Methods. The two-orbital double-exchange model with both the NN superexchange and electron-lattice coupling is here employed for the manganite bilayer components.²⁷ The effects of the FE P and polar layers are modeled by an electrostatic potential.²⁵ A $6 \times 6 \times 2$ cluster is used to simulate the manganite bilayer. In-plane “twisted” boundary conditions (BCs) are adopted in the zero-temperature (T) self-consistent calculations to reduce finite-size effects,³⁰ while periodic BCs are used in the computer time-consuming finite- T Monte Carlo (MC) simulations. The average e_g electronic density ($\langle n \rangle$) in the manganite bilayer is chosen as 0.7083, corresponding to a regime that typically has a FM ground state in manganites. All energies will be in units of t_0 , the double-exchange hopping amplitude (≈ 0.4 – 0.5 eV for LSMO).^{25,27} In addition, density functional theory (DFT) calculations were performed on the BaTiO₃-LSMO SL using the Vienna *ab initio* simulation package (VASP).^{31,32} Details of the model Hamiltonian and numerical methods are in the Supplemental Material.³³

Zero- T self-consistent calculation. First, the electrostatic potentials affecting the e_g electrons and the associated e_g

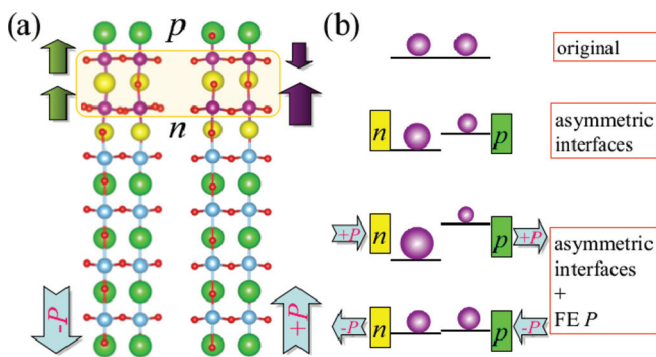


FIG. 2. (Color online) (a) Sketch of crystal structure.²⁹ Green = D; red = O; cyan = Ti; purple = Mn; yellow = $R_{1-x}A_x$. The n - p -type interfaces are indicated. Left/right are the $-P$ / $+P$ cases, with switched magnetic orders (FM/AF). (b) The e_g density (spheres) and potential (bars) modulated by asymmetric interfaces (bricks) and FE P (arrows).

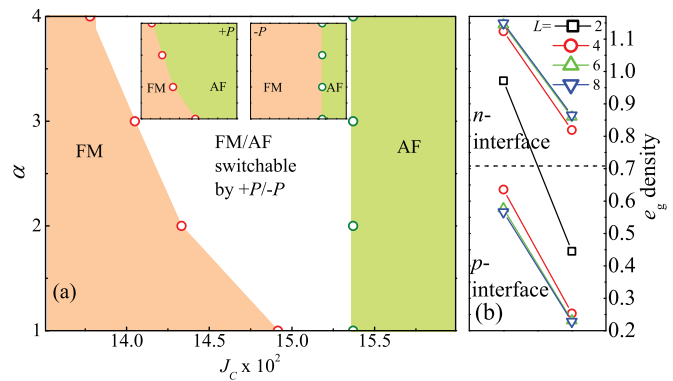


FIG. 3. (Color online) Zero- T model simulation results. (a) The ground-state phase diagram of manganite bilayers under $\pm P$. The middle (white) region is magnetically switchable by the FE P . Insets: phase diagrams under $+P$ (left) and $-P$ (right). The dielectric constant ϵ is represented by a Coulombic coefficient $\alpha \sim 1/\epsilon$ ($\alpha = 1$ corresponds to $\epsilon = 90$).³³ (b) The $+P$ modulated electronic densities of two interfacial layers with various manganite lengths (L). Dashed line: the original density. For all large L (>2) cases, the n -type interfaces own “high + high” density profiles while they are “low + low” for the p -type ones, which can resemble phase transitions in bulks. For only the $L = 2$ case, the density profile is “high + low,” which cannot be mapped directly to the bulk’s phase diagram.

densities (n_i ; i is the layer index) are calculated at $T = 0$ self-consistently via the Poisson equation and the model Hamiltonian. Then, the energies of the FM and AF states are compared to determine the ground state under $\pm P$. As shown in Fig. 3(a), in the $-P$ case the ground state is FM if the interlayer superexchange coupling J_c is smaller than 0.153. In the $+P$ case, the ground state is AF for a J_c larger than specific values that depend on the dielectric constant (ϵ) of manganite bilayers, all lower than 0.153 for all ϵ 's studied here. Therefore, within the middle region the magnetic ground state can switch from FM to AF by switching the direction of the FE P . Strictly speaking, here the AF order is ferrimagnetic once the magnetic moments from the e_g electrons are taken into account, since $n_1 > n_2$. Thus, the magnetic switch occurs between a FM state with strong M_{FM} and an AF state with a much weaker M_{AF} . Even with this caveat, the variation in M created by the P switch remains quite significant: $1 - M_{\text{AF}}/M_{\text{FM}} = 1 - [(3 + n_1) - (3 + n_2)]/[(3 + n_1) + (3 + n_2)] = 92\%$ ideally.

It is interesting to compare the magnetic switch effects described here against the interfacial phase transitions studied in thick manganite-FE heterostructures.^{23–26} As shown in Fig. 3(b), in thick manganite layers the local electronic densities of the first two interfacial layers can both be substantially enhanced or suppressed by the field effect. Then, the exchange coupling between the first two interfacial layers can be intuitively guessed from the bulk’s phase diagram. For example, if the local densities of both layers are close to unity, it is natural to expect locally an A-type AF state.²⁷ By contrast, this expectation is unrealistic in the bilayer case, since once n_1 is close to unity then n_2 must be close to or below 0.5. In this sense, the FE field effect in the bilayers is anomalous, with strong interference effects between the n - p - interfaces. And the magnetic coupling between the $n_1 \approx 1$ and $n_2 \approx 0.5$ layers

is unclear *a priori*. Thus, in spite of similarities, the underlying mechanism of the magnetic switch in the bilayers studied here is not qualitatively the same as for the phase transitions reported in thicker cases. Furthermore, due to the compensation effect between the neighboring *n*- and *p*-type interfaces, the charge modulation and electrostatic potential between the top and bottom layers in bilayers are obviously weaker than for thicker cases (more details in the Supplemental Material).³³

Finite-*T* MC simulation. The calculations described thus far relied on the comparison of energies between the ideal FM and AF phases, which is intuitively correct but needs confirmation using more powerful many-body techniques. In the following, finite-*T* MC simulations will be employed to confirm the previous results. The electron-phonon coupling is also taken into account in the MC simulation. Here the electron-phonon coupling coefficient is chosen as 1.2 and the superexchange coefficients as $J_{ab} = 0.07$ in-plane and $J_c = 0.14$ out-of-plane, which are realistic values from previous studies of manganites.^{25,27}

In this more rigorous approach, the switch from FM to AF states is still observed. Figure 4(a) shows the layer-resolved in-plane spin structure factors at wave vector (0,0) corresponding to in-plane FM order. All curves show paramagnetic (PM) to FM transitions although at different T_C 's. In the $-P$ case, the two layers transit synchronously since the electronic density is uniform. By contrast, in the $+P$ case, the two layers transit separately. Thus, in the mid-*T* region, the first layer becomes FM, but the second layer remains PM.

The averaged NN spin correlations between layers are shown in Fig. 4(b). Clearly, with decreasing *T* the $+P$ and $-P$

cases show opposite tendencies (AF vs FM coupling). Thus, the transitions revealed in Fig. 4(a) are PM-FM for the $-P$ case but PM-AF (ferrimagnetic) for the $+P$ case. The average *M*'s of the t_{2g} textures are presented in Fig. 4(c), which also display a clear contrast. In the $-P$ case, there is a peak in *M* in the mid-*T* region suggesting a ferrimagnetic transition, with a small but nonzero *M* up to low temperatures.

The T_C 's observed in these MC simulations are quite high. For a rough estimation, if the T_C of the bilayer (≈ 0.09) in the $-P$ case is used to fit the T_C (≈ 375 K) corresponding to LSMO ($x \approx 0.3$),²⁷ the upper-limit working *T* (≈ 0.07 – 0.08) for the magnetic switch can reach up to 290–330 K. Also, if the energy unit t_0 is estimated to be ≈ 0.4 – 0.5 eV for LSMO,²⁷ the upper-limit working *T* grows to 310–380 K. Both these estimations suggest that our proposed setup works at room *T*. Of course, finite-size extrapolations are difficult via time-consuming MC techniques.

Compared with the $T = 0$ self-consistent calculation using two preset candidate phases, the unbiased finite-*T* MC simulation is more reliable. For example, in our MC simulation, the robust electron-phonon coupling is essential to stabilizing the AF phase while it is not required in the $T = 0$ self-consistent case. In bulk undoped manganites such as LaMnO₃, the staggered $3x^2 - r^2/3y^2 - r^2$ orbital order (OO) associated with the Jahn-Teller distortion is prominent and crucial for the A-type AF state.^{27,34} This OO also plays an important role here in the bilayers. As shown in Figs. 4(d) and 4(e), the $+P$ case displays different OOs for the two layers. The first layer, which is close to the undoped case, shows the $3x^2 - r^2/3y^2 - r^2$ -like OO [Fig. 4(d)]. However, in the second layer, with an average electronic density slightly below 0.5, another type of OO is present which agrees with the $x^2 - y^2$ -type OO [Fig. 4(e)] known to exist in half-doped manganites.^{27,34} Both these two OOs have strong orbital lobes lying in-plane, which enhance (suppress) the in-plane (out-of-plane) double-exchange processes. Thus, this hybrid OO combination is advantageous to stabilizing the AF order in such a bilayer. By contrast, the $-P$ case shows uniform orbital occupancy [Fig. 4(f)], which prefers the FM state.

DFT study. The model simulations described above have been carried out in the ideal $-P$ limit (i.e., with full compensation between FE *P* and polar interfaces). However, as stated before, our predictions are not restricted by this condition. To confirm the robustness of our proposal, a preliminary *ab initio* DFT calculation was performed to verify the FE control of magnetic order.

The (BaTiO₃)₄-(LSMO)₂ ($x = 1/4$) SL was studied as the model system, as sketched in Fig. 2(a). According to the model study described above, an anisotropic superexchange is necessary for a switch function. In the DFT study, an in-plane tensile strain (for manganite) can induce such an effect. Thus, here the in-plane lattice constant of the SL is fixed to be 3.989 Å to fit the KTaO₃ substrate,³⁵ which can provide tensile strain to the LSMO bilayer. As shown in Table I, the calculated energies indicate that the ground state is FM under the $-P$ condition, but it switches to the AF state by using $+P$. The local magnetic moments also show a significant modulation in magnitude, implying the cross impact of the FE *P* and polar interfaces combination. The nonzero net *M* of the AF state in the DFT study suggests a ferrimagnetic state. In spite of

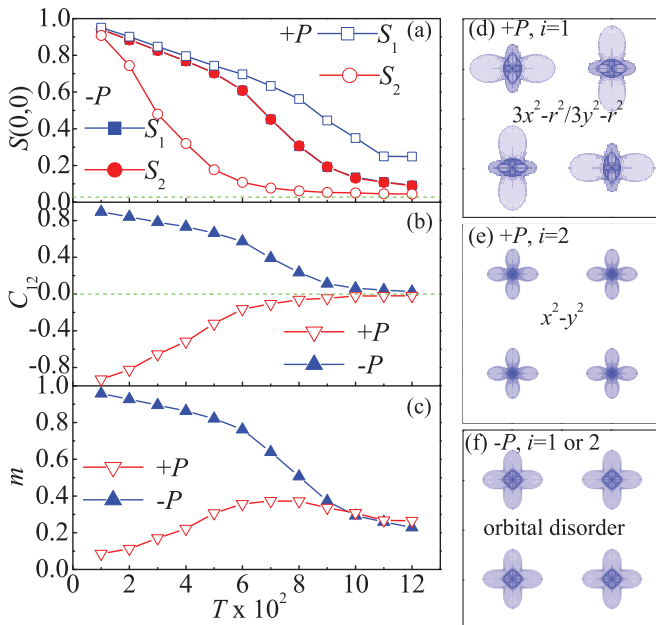


FIG. 4. (Color online) Results of MC simulations varying *T* for both $\pm P$. (a) Normalized spin structure factor at wave vector (0,0) (corresponding to a FM order) for each layer. (b) Average NN spin correlation (C_{12}) between two layers. (c) Normalized *M* (*m*) of the t_{2g} spin textures. (d)–(f) Orbital patterns (top view) obtained from MC simulations at $T = 0.01$. The size of the orbital lobes is proportional to the local electronic density.

TABLE I. DFT results. The first two columns specify the initial conditions. The energy differences (per Mn) between the FM (reference state) and AF orders are in meV units. m_1 and m_2 denote the local magnetic moment for the Mn cations using Wigner-Seitz spheres as specified by VASP which is not accurate but qualitatively preferable. M is the net magnetization. All moments are in μ_B/Mn units. The modulation of local magnetic moment is almost identical to the modulation of local electron density due to the half-metal character of LSMO.

| FE | Order | Energy | m_1 | m_2 | M |
|----|-------|--------|-------|--------|--------|
| +P | FM | 0 | 3.485 | 3.116 | 3.692 |
| +P | AF | -13.15 | 3.421 | -3.080 | 0.227 |
| -P | FM | 0 | 3.274 | 3.577 | 3.752 |
| -P | AF | 21.43 | 3.144 | -3.571 | -0.242 |

this caveat, the FM state displays a much larger net M , giving rise to a 93.9% modulation by switching P , in agreement with the model calculations described above. Then, the DFT study also confirms the FE control of magnetism, despite the modifications of the e_g density and the use of a nonideal $-P$ condition. More details of our DFT study can be found in the Supplemental Material.³³

Note. Finally, it is important to remark that although the notorious “dead layer” problem in real ultrathin manganite films may suppress ferromagnetism significantly,^{36,37} recent experiments indicate that the dead layers of LSMO should

be thinner than 2 u.c. per interface in the SL geometries.^{38,39} The latest experiments and theoretical simulations also show that local nonstoichiometry is responsible for dead layers.^{40–42} Thus, with further improvements in the fabrication techniques, “live” manganite bilayers in SLs will be possible, as designed in our model. Recent experimental and theoretical progress in the dead layer issue is shown in the Supplemental Material.³³

In summary, our theoretical studies, using both models and *ab initio* methods, predict the full control of magnetism when manganite bilayers are coupled to FE polarizations. The combination of FE polarization and asymmetric polar interfaces gives rise to two competing magnetic states: ferromagnetic and ferrimagnetic ones. The change of the total magnetization is remarkable (up to $\sim 90\%$) and may persist to room temperatures. Although our study uses titanates as the FE layers, the physical mechanism is general and applicable to other ferroelectrics. Similar effects are expected when using manganites at other doping concentrations and with other bandwidths, increasing the range of compounds where our proposal can be realized. Therefore, our work provides a potential design for pursuing the full control of magnetism in oxide heterostructures.

Acknowledgments. S.D. was supported by the 973 Projects of China (2011CB922101), NSFC (11004027, 11274060), NCET, and RFDP. E.D. was supported by the U.S. DOE, Office of Basic Energy Sciences, Materials Sciences and Engineering Division.

¹R. Ramesh and N. A. Spaldin, *Nat. Mater.* **6**, 21 (2007).

²C. A. F. Vaz, *J. Phys.: Condens. Matter* **24**, 333201 (2012).

³H. Y. Hwang, Y. Iwasa, M. Kawasaki, B. Keimer, N. Nagaosa, and Y. Tokura, *Nat. Mater.* **11**, 103 (2012).

⁴Y.-H. Chu, L. W. Martin, M. B. Holcomb, M. Gajek, S.-J. Han, Q. He, N. Balke, C.-H. Yang, D. Lee, W. Hu, Q. Zhan, P.-L. Yang, A. Fraile-Rodríguez, A. Scholl, S. X. Wang, and R. Ramesh, *Nat. Mater.* **7**, 478 (2008).

⁵H. Béa, M. Bibes, F. Ott, B. Dupé, X.-H. Zhu, S. Petit, S. Fusil, C. Deranlot, K. Bouzehouane, and A. Barthélémy, *Phys. Rev. Lett.* **100**, 017204 (2008).

⁶S. W. Wu, S. A. Cybart, P. Yu, M. D. Rossell, J. X. Zhang, R. Ramesh, and R. C. Dynes, *Nat. Mater.* **9**, 756 (2010).

⁷X. He, Y. Wang, N. Wu, A. N. Caruso, E. Vescovo, K. D. Belashchenko, P. A. Dowben, and C. Binek, *Nat. Mater.* **9**, 579 (2010).

⁸V. Laukhin, V. Skumryev, X. Martí, D. Hrabovsky, F. Sánchez, M. V. García-Cuenca, C. Ferrater, M. Varela, U. Lüders, J. F. Bobo, and J. Fontcuberta, *Phys. Rev. Lett.* **97**, 227201 (2006).

⁹S. Dong, K. Yamauchi, S. Yunoki, R. Yu, S. Liang, A. Moreo, J.-M. Liu, S. Picozzi, and E. Dagotto, *Phys. Rev. Lett.* **103**, 127201 (2009).

¹⁰S. Dong, Q. F. Zhang, S. Yunoki, J.-M. Liu, and E. Dagotto, *Phys. Rev. B* **84**, 224437 (2011).

¹¹Y. Shiota, T. Nozaki, F. Bonell, S. Murakami, T. Shinjo, and Y. Suzuki, *Nat. Mater.* **11**, 39 (2012).

¹²W.-G. Wang, M. Li, S. Hageman, and C. L. Chien, *Nat. Mater.* **11**, 64 (2012).

¹³A. Mardana, S. Ducharme, and S. Adenwalla, *Nano Lett.* **11**, 3862 (2011).

¹⁴M. Gajek, M. Bibes, S. Fusil, K. Bouzehouane, J. Fontcuberta, A. Barthélémy, and A. Fert, *Nat. Mater.* **6**, 296 (2007).

¹⁵V. Garcia, M. Bibes, L. Bocher, S. Valencia, F. Kronast, A. Crassous, X. Moya, S. Enouz-Vedrenne, A. Gloter, D. Imhoff, C. Deranlot, N. D. Mathur, S. Fusil, K. Bouzehouane, and A. Barthélémy, *Science* **327**, 1106 (2010).

¹⁶D. Pantel, S. Goetze, D. Hesse, and M. Alexe, *Nat. Mater.* **11**, 289 (2012).

¹⁷C. H. Ahn, A. Bhattacharya, M. D. Ventra, J. N. Eckstein, C. D. Frisbie, M. E. Gershenson, A. M. Goldman, I. H. Inoue, J. Mannhart, A. J. Millis, A. F. Morpurgo, D. Natelson, and J.-M. Triscone, *Rev. Mod. Phys.* **78**, 1185 (2006).

¹⁸C. A. F. Vaz, J. Hoffman, Y. Segal, J. W. Reiner, R. D. Grober, Z. Zhang, C. H. Ahn, and F. J. Walker, *Phys. Rev. Lett.* **104**, 127202 (2010).

¹⁹C. A. F. Vaz, Y. Segal, J. Hoffman, R. D. Grober, F. J. Walker, and C. H. Ahn, *Appl. Phys. Lett.* **97**, 042506 (2010).

²⁰L. Jiang, W. S. Choi, H. Jeon, T. Egami, and H. N. Lee, *Appl. Phys. Lett.* **101**, 042902 (2012).

²¹P. M. Leufke, R. Kruk, R. A. Brand, and H. Hahn, *Phys. Rev. B* **87**, 094416 (2013).

²²Y. W. Yin, J. D. Burton, Y. Kim, A. Y. Borisevich, S. J. Pennycook, S. M. Yang, T. W. Noh, A. Gruverman, X. G. Li, E. Y. Tsymlal, and Q. Li, *Nat. Mater.* **12**, 397 (2013).

²³J. D. Burton and E. Y. Tsymlal, *Phys. Rev. Lett.* **106**, 157203 (2011).

- ²⁴J. D. Burton and E. Y. Tsymbal, *Phys. Rev. B* **80**, 174406 (2009).
- ²⁵S. Dong, X. T. Zhang, R. Yu, J.-M. Liu, and E. Dagotto, *Phys. Rev. B* **84**, 155117 (2011).
- ²⁶H. Chen and S. Ismail-Beigi, *Phys. Rev. B* **86**, 024433 (2012).
- ²⁷E. Dagotto, T. Hotta, and A. Moreo, *Phys. Rep.* **344**, 1 (2001).
- ²⁸N. Nakagawa, H. Y. Hwang, and D. A. Muller, *Nat. Mater.* **5**, 204 (2006).
- ²⁹K. Momma and F. Izumi, *J. Appl. Crystallogr.* **41**, 653 (2008).
- ³⁰S. Dong, Q. F. Zhang, S. Yunoki, J.-M. Liu, and E. Dagotto, *Phys. Rev. B* **86**, 205121 (2012).
- ³¹G. Kresse and J. Hafner, *Phys. Rev. B* **47**, 558 (1993).
- ³²G. Kresse and J. Furthmüller, *Phys. Rev. B* **54**, 11169 (1996).
- ³³ See Supplemental Material at <http://link.aps.org/supplemental/10.1103/PhysRevB.88.140404> for further details.
- ³⁴T. Hotta, *Rep. Prog. Phys.* **69**, 2061 (2006).
- ³⁵Some other combinations of substrates, manganites, and titanates have also been tested. A proper in-plane tensile is important to tune the subtle balance between the FM and AF orders, namely, the switching function.
- ³⁶M. Huijben, L. W. Martin, Y.-H. Chu, M. B. Holcomb, P. Yu, G. Rijnders, D. H. A. Blank, and R. Ramesh, *Phys. Rev. B* **78**, 094413 (2008).
- ³⁷A. Tebano, C. Aruta, S. Sanna, P. G. Medaglia, G. Balestrino, A. A. Sidorenko, R. De Renzi, G. Ghiringhelli, L. Braicovich, V. Bisogni, and N. B. Brookes, *Phys. Rev. Lett.* **100**, 137401 (2008).
- ³⁸L. F. Kourkoutis, J. H. Song, H. Y. Hwang, and D. A. Muller, *Proc. Natl. Acad. Sci. USA* **107**, 11682 (2010).
- ³⁹A. X. Gray, C. Papp, B. Balke, S.-H. Yang, M. Huijben, E. Rotenberg, A. Bostwick, S. Ueda, Y. Yamashita, K. Kobayashi, E. M. Gullikson, J. B. Kortright, F. M. F. de Groot, G. Rijnders, D. H. A. Blank, R. Ramesh, and C. S. Fadley, *Phys. Rev. B* **82**, 205116 (2010).
- ⁴⁰R. Peng, H. C. Xu, M. Xia, J. F. Zhao, X. Xie, D. F. Xu, B. P. Xie, and D. L. Feng, arXiv:1301.4822.
- ⁴¹F. Song, F. Monsen, Z. S. Li, J. W. Wells, and E. Wahlström, *Surf. Interface Anal.* **45**, 1144 (2013).
- ⁴²C. Wang, N. Stojić, and N. Binggeli, *Appl. Phys. Lett.* **102**, 152414 (2013).